Presented at the 28th European PV Solar Energy Conference and Exhibition, 30 September – 4 October, 2013, Paris, France

MATERIAL LIMITATIONS DUE TO CRUCIBLE IMPURITIES IN MULTICRYSTALLINE SILICON FOR HIGH EFFICIENCY SOLAR CELLS

Florian Schindler [a,b], Bernhard Michl [a], Jonas Schön [a], Wolfram Kwapil [a,b], Wilhelm Warta [a], and Martin C. Schubert [a]
[a] Fraunhofer Institut für Solare Energiesysteme, Heidenhofstr. 2, D-79110 Freiburg, Germany
[b] Freiburger Materialforschungszentrum, Albert-Ludwigs-Universität Freiburg, Stefan-Meier-Str. 21, D-79104 Freiburg, Germany
Ph +49 761 4588 5321, Fax +49 761 4588 9250, Email: florian.schindler@ise.fraunhofer.de

ABSTRACT: For the fabrication of high efficiency silicon solar cells, bulk material with low recombination losses is required. Crystal defects and impurities from feedstock and crucible system harm the electrical material quality of multicrystalline silicon wafers. In this work, spatially resolved efficiency losses in multicrystalline silicon are estimated from injection-dependent bulk lifetime measurements, and the impact of decorated crystal defects, dissolved impurities and impurities diffused into the crystallized silicon by solid-state diffusion is quantified. The high-temperature steps of two solar cell processes, a standard PERC process and a high efficiency approach, are applied to two different p-type multicrystalline silicon materials: One block was crystallized in a G1 sized crucible of industrial material quality and the other in a crucible of very pure electrically fused silica. The high purity wafers allow higher efficiencies than the wafers from the standard crucible after both cell processes and profit from a larger efficiency boost achieved by the high efficiency process. An efficiency gain of 0.5% absolute is estimated to be attainable on wafers including a block edge by using a high purity crucible.
Keywords: Multicrystalline Silicon, Defects, Impurities

1 INTRODUCTION

While costs and energy consumption for the crystallization of multicrystalline (mc) silicon are lower than for monocrystalline silicon, the fabrication of high efficiency crystalline silicon solar cells is still limited to monocrystalline wafers due to its lower impurity content and the absence of crystal defects. Although feedstock quality and crystallization processes of mc silicon have improved significantly in recent years, its electrical material quality is still limited by metal impurities and crystal defects. The main sources for impurities are the quartz crucible and the crucible coating. In recent work, the role of crucible and coating on impurities in crystallized silicon has been investigated [1-5]. Impurities can diffuse into the liquid silicon melt and during the crystallization be incorporated into the crystal lattice leading to a background impurity concentration which increases towards the top of the crystal due to the very low segregation coefficients of metals. Additionally, solid-state diffusion from the crucible and its coating into the solidified part of the ingot takes place, leading to an edge region of very high impurity concentration and low bulk lifetimes. Both, the background impurity concentration and the high concentration in the edge region limit the bulk lifetime and thereby material quality of multicrystalline silicon. Improving the purity of the crucible and its coating is one approach to reach better electrical material quality and thereby higher efficiencies on multicrystalline silicon solar cells.

In this work, the influence of impurities from the crucible system on solar cell efficiency losses in multicrystalline silicon will be investigated. Therefore, the material related efficiency losses of wafers from a block that was crystallized by directional solidification in a standard crucible are compared to the losses of wafers from a block crystallized in a crucible of high purity. To separate the influence of the different crucible materials from other aspects affecting the material quality, the crystallizations were conducted under comparable conditions (temperature profiles, crystallization time, gas flows) in the same crystallization furnace, and a comparable crucible coating as well as the same silicon feedstock was used. Spatially resolved injection-dependent bulk lifetime measurements allow for an estimation of the bulk limited solar cell efficiency potential by the "Efficiency limiting bulk recombination analysis" (ELBA) [6]. The impact of iron is determined by the same approach based on spatially resolved measurements of the interstitial iron concentration. Two different cell processes are compared, a standard PERC process and a high efficiency PERC approach with an additional oxidation for front surface passivation.

2 MATERIAL AND METHODS

For our investigations, boron-doped p-type multicrystalline material from two G1 crystallizations (~220x220x128mm³) was used. The crystallizations differed only in the material quality of the crucibles, while the furnace and process recipe remained unchanged. One crystallization was realized in a crucible of standard industrial quality ("*SQ*"), the other one in a crucible of very high purity ("*HP*").

In this paper we focus on 125x62.5mm²-sized wafers, such that impurities diffused into the crystallized block by solid-state diffusion affect only one edge of the wafers (in the following referred to as "edge region"; the rest of the wafer, where no edge-influence on bulk lifetime is visible, is denoted as "central region").

Fig. 1 shows the high temperature processing steps of the different wafers: Two 125x62.5mm² sister wafers from a central block height of each ingot were subjected to all high temperature steps including phosphorous diffusion of two different cell processes ("PD" and "PD+Ox") and served as lifetime samples for cell simulations. The only difference between "PD" and "PD+Ox" is the oxidation at 840°C, which is applied to achieve better front surface passivation in the solar cell. For the lifetime samples, the oxide films and emitter layers were etched away prior to passivating the samples with Al_2O_3 in order to obtain lifetime samples with identically passivated surfaces. A third sister wafer from each ingot was

just chemically polished (CP etch) and passivated with Al_2O_3 to serve as an ungettered reference sample.

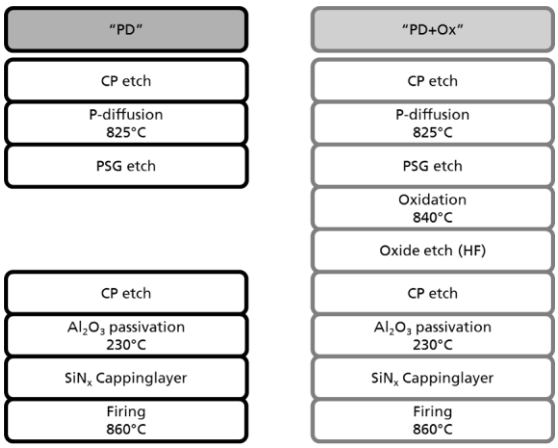

Figure 1: Sample Processing

The high temperature steps of "PD" correspond to those of a standard PERC process, while the additional oxidation in "PD+Ox" is part of a high efficiency PERC process with a lower front surface recombination based on the additional oxide-passivation.

Images of the injection-dependent minority charge carrier bulk lifetime and interstitial iron concentration [7] were obtained by means of QSSPL-calibrated photoluminescence imaging (PLI) [8]. The injection-dependent bulk lifetime images allow for an estimation of the bulk limited cell efficiency potential by the "Efficiency limiting bulk recombination analysis" (ELBA) [6] (with modifications described in [9]): Based on the injection-dependent bulk lifetime images, pseudo efficiency images are calculated via PC1D models. The cell structure is a passivated emitter and rear LFC cell with a honeycomb texture. The front, emitter and back side recombination parameters and optics for the PC1D model "PD+Ox" are taken from reference [10]. In [10] the model was adjusted to measurements of external and internal quantum efficiency and reflection of a honeycomb textured LFC cell that featured also the "PD+Ox" front side. The emitter saturation current density J_{0e} calculated from J_{sc} and V_{oc} is 180 fA/cm² for the "PD+Ox" model. The "PD" model differs only from the "PD+Ox" model in the front and emitter recombination. These were adjusted to a J_{0e} of 630 fA/cm² measured on honeycomb textured samples with SiN_x passivated emitter without oxidation. The higher value reflects the missing oxide passivation and the missing improvements of the emitter profile during the oxidation, which is especially important for a honeycomb texture due to the large surface area. The base doping of the cell models is taken from the mc samples, $1.4x10^{16}cm^{-3}$ for the *SQ*-material and $1.7x10^{16}cm^{-3}$ for the *HP*-material. This allows for a calculation of the pseudo-efficiency limit of the cells (limit due to the cell concept neglecting series resistance losses and bulk recombination, in the following termed "cell limit"): The pseudo-efficiency limit of "PD" is 20.0% for both materials; the limit of "PD+Ox" is slightly higher for the *HP*-wafers (21.3%) than for the *SQ*-wafers (21.2%). This is due to the higher doping of the *HP*-wafers and thus higher V_{oc} values and will be taken into account when discussing the material related losses in section 3.

3 RESULTS

3.1 Impact of solar cell processing on material quality

During the high temperature steps of a solar cell process, impurities in the bulk are redistributed. These effects are depicted in Fig. 2, showing the square root harmonic mean of the bulk lifetime at an illumination of 0.1 suns, and Fig. 3, showing the averaged interstitial iron concentration, both in the central region of the wafers.

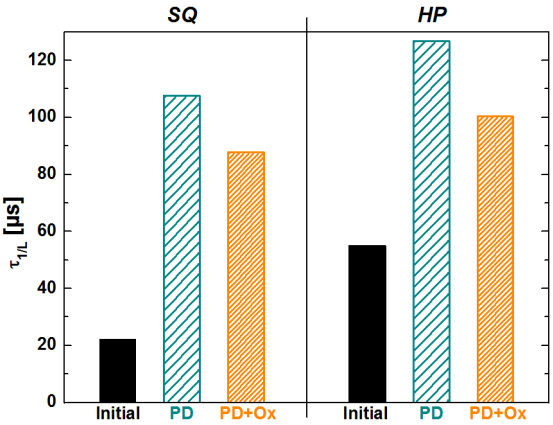

Figure 2: Averaged bulk lifetimes in the central region

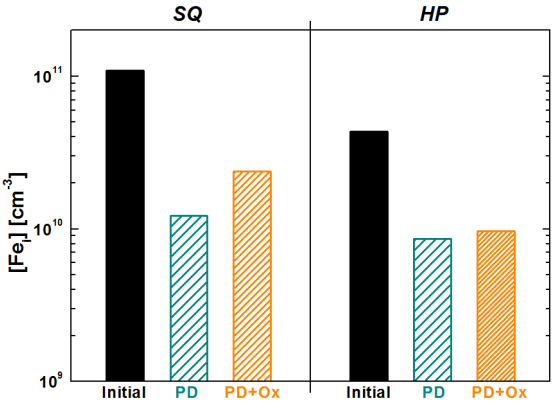

Figure 3: Averaged concentrations of interstitial iron in the central region

Bulk lifetime increases significantly during the phosphorous diffusion in both materials, which is attended by a decrease in the concentration of interstitial iron. Due to the efficient gettering of impurities, after the phosphorous diffusion the difference in material quality in the central region of *SQ*- and *HP*-wafers is smaller than in the as-cut state. Both materials suffer from the subsequent oxidation step, which is reflected in a decrease of the bulk lifetime and an increase of the interstitial iron concentration. This high temperature step can dissolve iron-precipitates and iron-agglomerations at crystal defects, formed during the crystallization, and leads to a back-diffusion of previously gettered iron from the phosphorous layer into the silicon bulk.

3.2 Bulk limited cell efficiency potential

As discussed in the previous section, the additional oxidation harms the material quality of mc wafers. On the other hand, the oxidation leads to a significantly better front surface passivation in the solar cell.

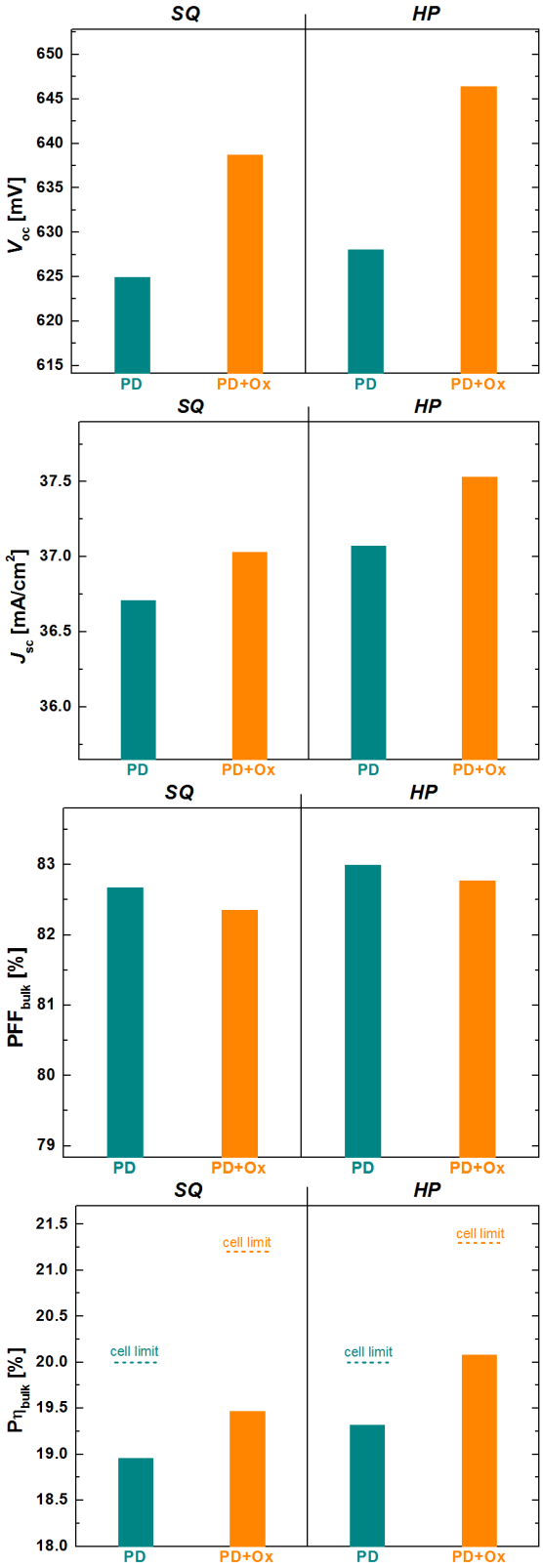

Figure 4: V_{oc}, J_{sc}, PFF_{bulk} and $P\eta_{bulk}$ after two different cell processes in the *SQ*-material (left) and the *HP*-material (right)

Hence, for a prediction of cell performances, material limitations as well as limitations due to the cell concept have to be taken into account. This is done in the following by an "Efficiency limiting bulk recombination analysis" (ELBA) [6, 9], which combines measurements of spatially resolved and injection-dependent bulk lifetime with a cell simulation based on PC1D as explained in section 2. Modeling the open-circuit voltage V_{oc}, the short-circuit current J_{sc}, the pseudo fill factor PFF_{bulk} (neglecting series resistance losses, only lower than ideal fill factor due to injection-dependent bulk recombination) and the pseudo efficiency $P\eta_{bulk}$ (neglecting series resistance losses) from the injection-dependent bulk lifetimes and averaging across the wafer delivers the results depicted in Fig. 4. In combination with the spatially resolved simulated pseudo efficiency $P\eta_{bulk}$, these values can be discussed in detail. Figure 5a) shows $P\eta_{bulk}$ for the *SQ*-wafer, figure 5b) for the *HP*-wafer. The left half of the images refers to the cell process without oxidation, the right half to the high efficiency cell process.

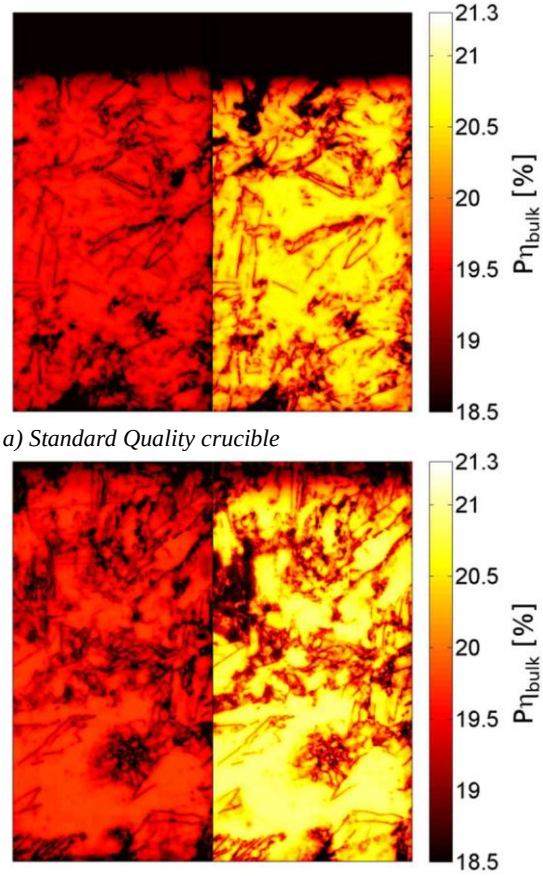

a) Standard Quality crucible

b) High Purity crucible

Figure 5: Spatially resolved $P\eta_{bulk}$ (from reference [11]). The left half of the images refers to the cell process without oxidation ("PD"), the right half with the additional oxidation ("PD+Ox")

Both materials benefit from the additional front surface passivation, which leads to a strong increase in V_{oc} (cf. 1st graph of Fig. 4) which is visible in a homogeneous increase in efficiencies in the good grains. On the other hand, the increase in J_{sc} is smaller and PFF_{bulk} even decreases after the additional oxidation due to the material degradation during the high temperature step. We showed in reference [11] that the bulk lifetime in regions of low material quality like the edge region or dislocation clusters features a strong injection dependence. As the injection conditions at J_{sc} and MPP are significantly lower than at V_{oc}, the global values of J_{sc} and PFF_{bulk} especially suffer from the material degradation after oxida-

tion in these regions. Fig. 6 highlights this effect: J_{sc}-losses after oxidation are particularly high in regions of low material quality.

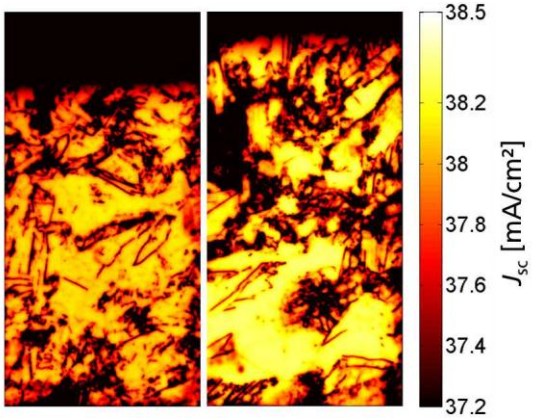

Figure 6: J_{sc} after the cell process with oxidation ("PD+Ox") in the standard quality material (left) and the high purity material (right)

These results show the double-edged impact of the high efficiency solar cell process "PD+Ox": While V_{oc} benefits strongly from the additional oxide passivation on the front side, the benefit in J_{sc} is smaller and PFF_{bulk} even decreases due to the lower material quality after the high temperature step. In combination, the high efficiency cell process leads to a raise in pseudo efficiency from 19.0% to 19.5% for the *SQ*-material and from 19.3% to 20.1% for the *HP*-material (cf. Fig. 4). Due to the better material quality of the *HP*-wafers, the efficiency boost obtained by "PD+Ox" on these wafers (+0.8% abs.) is larger than on the *SQ*-wafers (+0.5% abs). This elucidates the benefit of crucibles of higher purity: While for the standard cell process the difference in material quality is less critical for solar cell efficiencies, it becomes more important for high efficiency cell processes.

In a last step, we discuss the origin of the efficiency losses after the high temperature oxidation in detail. To this aim, we evaluated the efficiency potential in the best 1x1cm² area which is virtually free of crystal defects in both materials. The loss compared to the cell limit can be attributed to dissolved impurities that diffused into the liquid silicon melt before crystallization and remained after processing (first (orange) part of the columns in Fig. 7). To assess the influence of crystal defects such as dislocations and grain boundaries, in a second step the efficiency potential in the central region (without any edge influence) is evaluated. The additional loss can then be attributed to recombination via impurities at dislocations and grain boundaries (second (cyan) part of the columns in Fig. 7). In a last step, by evaluating the efficiency potential of the whole wafer, also the edge region and therefore the efficiency loss due to impurities diffused into the crystal by solid-state diffusion is taken into account (third (grey) part of the columns in Fig. 7). Fig. 7 shows relative efficiency losses referring to the cell limit.

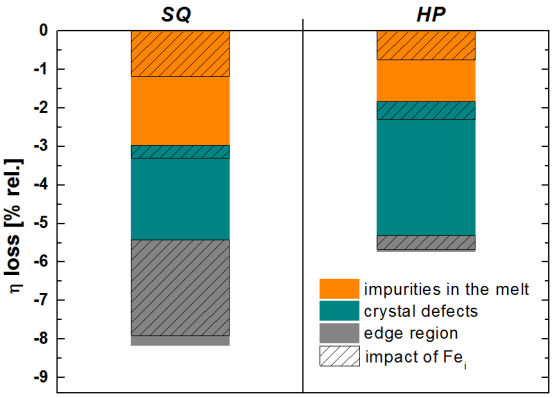

Figure 7: Relative efficiency losses after the cell process with oxidation ("PD+Ox") in the standard quality material (left) and the high purity material (right)

The main losses in the *SQ*-material are remaining dissolved impurities which had diffused into the melt before crystallization (-3.0% rel.) and impurities diffused into the solidified crystal by solid-state diffusion visible in the large edge region (width on the wafer ~25mm; -2.7% rel.). In contrast, in the *HP*-material the main losses can be attributed to recombination active crystal defects like dislocation clusters and grain boundaries (-3.5% rel.). In total the losses sum up to -8.2% rel. in the *SQ*-material and -5.7% rel. in the *HP*-material, leading to a significantly higher efficiency potential in the *HP*-material of 20.1% compared to 19.5% in the *SQ*-material. As the losses in the HP-material related to decorated crystal defects are even higher than in the SQ-material (*HP*: -3.5% rel.; *SQ*: -2.5% rel.), the benefit from purer crucible materials could be even stronger if the crystal quality of both materials was comparable. In this specific case, the same temperature profiles for crystallization were used for *SQ* and *HP* without optimizing the profile for the thinner *HP* crucible. This might be a reason for the lower crystal quality of the *HP*-material. In general, using a high purity crucible should not impact the crystal quality if the temperature profiles were adapted to the thinner crucible.

With the help of measured images of interstitial iron concentrations, we can now evaluate the impact of interstitial iron on cell level. To do so, we performed the same simulations as above with the measured concentration of interstitial iron as the only bulk lifetime limiting recombination channel (input for cell simulation: injection dependent images of $\tau_{SRH,Fei}$). The result can be seen in Fig. 7 as the shaded fractions of the columns, which express the corresponding relative efficiency losses due to interstitial iron. A major part of the losses due to dissolved impurities that had diffused into the melt can be attributed to interstitial iron (~40% for both materials); losses due to the edge region are even dominated by interstitial iron (~90%). In contrast, interstitial iron plays a minor role for losses due to decorated defects. However, these losses might also be attributed to iron or iron precipitates bound to crystal defects.

4 CONCLUSIONS

In this work we show for G1 sized crucibles that efficiency losses in multicrystalline silicon can be reduced by crystallizing the silicon in crucibles of pure material quality (here electrically fused silica). While the difference in material quality of wafers from a standard quality

crucible and wafers from a high purity crucible is less critical for a standard solar cell process, the benefit of the high purity crucible is especially notable in solar cell efficiencies after a high efficiency solar cell process comprising a high temperature oxidation. In the high purity wafers, the loss in good grains due to remaining dissolved impurities that had diffused into the silicon melt is reduced by around 40% compared to the standard quality material. Additionally, the wider edge region in material from standard quality crucibles plays a crucial role, in our case losses due to the edge region are reduced by 85% in the material from the high purity crucible, mainly because the size of the edge region on the wafers decreases from about 25mm to 6mm. However, as the crystal structure of the material from the standard crucible is better under the crystallization conditions chosen, losses due to decorated crystal defects are larger in the material from the high purity crucible. This should be avoidable by applying a crystallization process adapted to the thermal properties of the crucible. Limitations like crystal defects decorated with metal impurities indicate that besides a high purity crucible also a crucible coating of highest purity has to be used to reduce the impurity transport from the crystallization environment into the silicon bulk as far as possible.

In industry, larger crucibles of up to 1000 kg of silicon (G6) are used. On the basis of the experimentally validated simulations our results on G1 blocks (14 kg) can be transferred directly to these ingot sizes [5]. Our general conclusions remain valid as the major part of the wafers will still be influenced by the edge region (20 of 36 wafers in G6 are “edge wafers”) and the edge region itself even becomes wider. However, the width of the edge region in the wafers depends strongly on the fraction cut off from the entire block. Further details on the transfer to larger crucible sizes can be found in [5].

Additionally, we elaborated the role of interstitial iron and showed that it plays a major role for losses due to dissolved impurities and dominates the losses in the edge region. At crystal defects other impurities than interstitial iron are dominating the losses, which may well be iron precipitates or iron bound to dislocations or grain boundaries.

ACKNOWLEDGEMENTS

This work was financially supported by the German Federal Ministry for the Environment, Nature Conservation and Nuclear Safety and by industry partners within the research cluster “SolarWinS” (contract No. 0325270G). The content is the responsibility of the authors.

REFERENCES

[1] B. Geyer, G. Schwichtenberg, and A. Muller, presented at the Proceedings of the 31st IEEE Photovoltaic Specialists Conference, Orlando, Florida, USA, 2005 (unpublished).

[2] E. Olsen and E. J. Øvrelid, Progress in Photovoltaics: Research and Applications **16** (2), 93 (2008).

[3] T. Naerland, L. Arnberg, and A. Holt, Progress in Photovoltaics: Research and Applications **17** (5), 289 (2009).

[4] R. Kvande, L. Arnberg, and C. Martin, Journal of Crystal Growth **311** (3), 765 (2009).

[5] M. C. Schubert, J. Schön, F. Schindler, W. Kwapil, A. Abdollahinia, B. Michl, S. Riepe, C. Schmid, M. Schumann, S. Meyer, and W. Warta, Journal of Photovoltaics **in press, DOI: 10.1109/ JPHOTOV.2013.2279116** (2013).

[6] B. Michl, M. Rüdiger, J. Giesecke, M. Hermle, W. Warta, and M. C. Schubert, Solar Energy Materials & Solar Cells **98**, 441 (2012).

[7] D. Macdonald, J. Tan, and T. Trupke, Journal of Applied Physics **103**, 073710 (2008).

[8] J. A. Giesecke, M. C. Schubert, B. Michl, F. Schindler, and W. Warta, Solar Energy Materials and Solar Cells **95** (3), 1011 (2011).

[9] B. Michl, M. Kasemann, W. Warta, and M. C. Schubert, Physica Status Solidi - rapid research letters **published online, DOI 10.1002/ pssr.201308090** (2013).

[10] H. Hauser, B. Michl, S. Schwarzkopf, V. Kübler, C. Müller, M. Hermle, and B. Bläsi, IEEE Journal of Photovoltaics **2** (2), 114 (2012).

[11] F. Schindler, B. Michl, J. Schön, W. Kwapil, W. Warta, and M. C. Schubert, Journal of Photovoltaics **accepted** (2013).